World Academy of Science, Engineering and Technology
International Journal of Chemical and Molecular Engineering
Vol:13, No:6, 2019

Comparative Study of Calcium Content on *in vitro* Biological and Antibacterial Properties of Silicon-Based Bioglass

Morteza Elsa, Amirhossein Moghanian

Abstract**—**The major aim of this study was to evaluate the effect of CaO content on *in vitro* hydroxyapatite formation, MC3T3 cells cytotoxicity and proliferation as well as antibacterial efficiency of sol-gel derived SiO_2–CaO–P_2O_5 ternary system. For this purpose, first two grades of bioactive glass (BG); BG-58s (mol%: 60%SiO_2–36%CaO–4%P_2O_5) and BG-68s (mol%: 70%SiO_2–26%CaO–4%P_2O_5)) were synthesized by sol-gel method. Second, the effect of CaO content in their composition on *in vitro* bioactivity was investigated by soaking the BG-58s and BG-68s powders in simulated body fluid (SBF) for time periods up to 14 days and followed by characterization inductively coupled plasma atomic emission spectrometry (ICP-AES), Fourier transform infrared spectroscopy (FTIR), X-ray diffraction (XRD), and scanning electron microscopy (SEM) techniques. Additionally, live/dead staining, 3-(4,5dimethylthiazol-2-yl)-2,5-diphenyltetrazolium bromide (MTT), and alkaline phosphatase (ALP) activity assays were conducted respectively, as qualitatively and quantitatively assess for cell viability, proliferation and differentiations of MC3T3 cells in presence of 58s and 68s BGs. Results showed that BG-58s with higher CaO content showed higher *in vitro* bioactivity with respect to BG-68s. Moreover, the dissolution rate was inversely proportional to oxygen density of the BG. Live/dead assay revealed that both 58s and 68s increased the mean number live cells which were in good accordance with MTT assay. Furthermore, BG-58s showed more potential antibacterial activity against methicillin-resistant *Staphylococcus aureus* (MRSA) bacteria. Taken together, BG-58s with enhanced MC3T3 cells proliferation and ALP activity, acceptable bioactivity and significant high antibacterial effect against MRSA bacteria is suggested as a suitable candidate in order to further functionalizing for delivery of therapeutic ions and growth factors in bone tissue engineering.

Keywords**—**Antibacterial, bioactive glass, hydroxyapatite, proliferation, sol-gel processes.

I. Introduction

BG is one of the main subgroup of osteoproductive biomaterials that well-known for their properties in bone tissue engineering [1], [2]. BGs are capable of bonding directly to surrounding bone tissue after implantation in the body by both formation the hydroxyapatite (HA) on the surfaces and ion release which stimulate bone cell proliferation [3], [4]. This bone bonding behavior of the BGs is known as bioactivity [5]. The first BG was synthesized in 46.1 SiO_2, 2.6 P_2O_5, 24.4 Na_2O, 26.9 CaO (in mol%), system through melt quenching technique by Hench in 1969 [6].

In melt quenching process, BGs were synthesized by the melting and mixing of oxides in compositions such as silica, calcium, phosphate, and sodium at high temperatures, which are typically from 1200 to 1500 °C depending on the BG composition. On the other hand, sol gel method was proposed in the last decade [7] which involves mixing the inorganic metal salts as a precursor [8].

BGs can be synthesized by sol-gel or traditional melt-quenching routs. Additionally, several advantages of sol-gel over melt quenching technique have been reported such as lower processing temperature, more purity and homogeneity due to less evaporation of P_2O_5 [9]–[12]. On the other hand, studies have also demonstrated that sol-gel-derived BGs have significantly faster *in vitro* HA formation in compared to the melt- derived BGs [13], [14].

The following five steps were suggested for the *in vitro* or in vivo formation of hydroxycarbonate apatite (HCA) on BGs surfaces in SBF or in body fluid, respectively [15], [16].

1. Creation of silanol (Si–OH) on the BG surface by rapid cation exchange of Ca^{2+} with H^+ from SBF.
2. Breakage the Si–O–Si bonds and formation the Si–OH at the interfaces of BG–SBF
3. Repolymerization of the silica-rich layer at BG surface by condensation of Si–OH groups.
4. Formation the amorphous CaO–P_2O_5 on the silica-rich layer with the migration of Ca^{2+} and PO_3^{-4} groups from SBF.
5. Crystallization of the CaO–P_2O_5 to HCA by incorporation of hydroxyls and carbonate from SBF.

Previously many grades of BGs with different chemical composition such as BG-58s, BG-68s, BG-77s, and etc. have been suggested for various biomedical applications such as dental, orthopaedic, and drug delivery in tissue engineering field [17]–[24]. Moreover, in the clinical applications of BGs, one of the most critical issues is bacterial infection which can be fatal after BG implantation in tissue engineering surgery [25]. MRSA, one of the serious bacteria, is an important cause of hospital acquired infections that have recently become more prevalent in the community [26]. Moreover, the antibacterial activity of BGs against wide range of bacteria has been previously suggested [27]–[29]. Therefore, from this point of view, considering the BG as an antibacterial agent is a

Morteza Elsa is with the Scientific and technology park, Imam Khomeini International University, Qazvin, 34149-16818, Iran (corresponding author, phone: +98 9123816103, fax: +09833901186, e-mail: mortez.elsa@gmail.com).

Amirhossein Moghanian is with the Scientific and technology park, Imam Khomeini International University, Qazvin, 34149-16818, Iran and Harvard-MIT Division of Health Sciences and Technology, Massachusetts Institute of Technology, Cambridge 02139, MA, USA.

promising method in implant-related surgery.

In recent years several studies have been performed on the synthesis, characterization, biological and antibacterial investigation of the sol–gel derived BGs in the system of SiO_2–CaO–P_2O_5 such as 58s and 68s BG [14], [30]–[35]. But, no comprehensive study has been conducted in order to investigate the effect of difference CaO content in 58s and 68s BGs on *in vitro* HA formation, biological and bacterial studies. Hence, the main aim of this study was to investigate the effect of CaO content on *in vitro* bioactivity, cytocompatibility and antibacterial efficiency of gel derived ternary BG. For this purpose, two BGs in SiO_2–CaO–P_2O_5 ternary system with different compositions (i.e. BG-58s (mol%: 60%SiO_2–36%CaO–4%P_2O_5) and BG-68s (mol%: 70%SiO_2–26%CaO–4%P_2O_5)) with the fixed phosphorus content were synthesized by sol-gel method. Then, the effect of Ca content on *in vitro* HA formation was studied by ICP-AES, FTIR, XRD and SEM. Moreover, staining techniques (i.e. L/D) and biological evaluations (i.e. MTT and ALP) were applied respectively as qualitatively and quantitatively assess for cell viability, differentiations and observation the morphology of the MC3T3's nuclei and actin fibers in presence of 58s and 68s BG. In addition, the bactericidal activities of synthesized BGs against MRSA bacteria were compared with the control by using colony-forming method. Eventually, according to the *in vitro* bioactivity, cell proliferation, ALP, antibacterial activity results, the most promising CaO content in the BG's with fixed 4 mol% P_2O_5 composition was suggested.

II. Materials and Method

A. BG and SBF Synthesis

Two 58s and 68s BG were synthesized through sol– gel method. The chemical compositions are given in Table I. Briefly, tetraethyl orthosilicate (TEOS: $Si(OC_2H_5)$) as a silicate precursor was mixed with water (hydrolysis) under acidic condition (0.1 M HNO_3) and followed by consecutive addition of triethylphosphate (TEP: $PO(OC_2H_5)_3$) and calcium nitrate ($Ca(NO_3)_2$,$4H_2O$) to form a transparent and homogenous sol. Afterwards, the sols were aged at 37 °C for 3 days, dried at 75 °C for 24 h and calcined at 700 °C for 3 h in a furnace to remove the organic substances and residual nitrate. Then, the obtained gel was milled in a planetary ball mill (Retsch, Germany) to reduce particle size below 50 μm, and then the powder was pressed to disc-shaped pellet (Ø10×3 mm) by applying 9 MPa pressure under a hydraulic press.

TABLE I
Elemental Compositions of the BG-58s and BG-68s (in Mol %)

glass	Label	SiO_2	CaO	P_2O_5
BG-58s	(58s)	60	36	4
BG-68s	(68s)	70	26	4

For the biological investigations, the SBF (the most similar solution to human blood plasma) was prepared based on the recipe proposed by Kokubo [11] by dissolving the reagent-grade $CaCl_2$ (calcium chloride), $K_2HPO_4.3H_2O$ (monopotassium phosphate), NaCl (sodium chloride), KCl (potassium chloride), $MgCl_2.6H_2O$ (magnesium chloride hexahydrate), $NaHCO_3$ (sodium bicarbonate), and Na_2SO_4 (sodium sulfate) in distilled water and adjusting the pH with Tris-buffer (tris hydroxymethyl aminomethane) and HCl (hydrochloric acid). All the chemicals were obtained from Sigma-Aldrich Co. and used without further purification.

Nominal ions concentrations of SBF in comparison with the human blood plasma are given in Table II.

TABLE II
Composition of SBF Solution and Human Blood Plasma (mmol L^{-1})

Ion	Plasma (mmol.L^{-1})	SBF (mmol.L^{-1})
Na^+	142.0	142.0
K^+	5.0	5.0
Mg^+	1.5	1.5
Ca^{+2}	2.5	2.5
Cl^-	103.0	147.8
HCO_3^-	27	4.2
HPO_4^{-2}	1.0	1.0
SO_4^{-2}	0.5	0.5

B. Characterization of BGs

1. Density Measurements and Calculation of Oxygen Density

The liquid displacement method was used to measure the density of the BG (ρ_{glass}) by immersing the BG powders in de-ionized water in a 25 ml pycnometer (Gay-Lussac, Germany) as previously described [36]. In addition, to evaluate the network connectivity in synthesized BGs and to compare their compactness, oxygen densities of 58s and 68s were calculated according to (1) [37]:

$$\rho_O = M_O \times \left(2x_{SiO_2} + x_{CaO} + 5x_{P_2O_5}\right) / \left[x_{SiO_2}M_{SiO_2} + x_{CaO}M_{CaO} + x_{P_2O_5}M_{P_2O_5}\right] \times \rho_{glass}^{-1} \quad (1)$$

where M_O is the atomic mass of oxygen; i.e. M_{SiO2} , M_{CaO} and M_{P2O5} are the molecular masses of SiO_2, CaO and P_2O_5, respectively. Moreover, $xSiO_2$, xCaO and xP_2O_5 are the molar fractions of SiO_2, CaO, and P_2O_5, respectively.

2. XRD, FTIR and SEM Analyses

HA formation was also analyzed by XRD (INEL-Equinox-3000, France) using Cu-Kα radiation (λ =1.5405 A°) within a 2θ range of 15°–40° at a scanning speed of 1.2 °/min. Additionally, the chemical structure of the formed HA on 58s and 68s surfaces was characterized using a FTIR spectroscopy (Nicolet Avatar 660, USA) in the wavenumber range of 400–4000 cm^{-1} with a resolution of 8 cm^{-1}.

SEM (Philips XL30, Netherland) was employed to observe the morphology of the formed HA on BGs surfaces over immersion time periods up to 14 days.

3. ICP-AES

The ion solubility investigation was done at 37 °C by soaking the tablets with a constant ratio of surface area (SA) to SBF volume (V) of 0.1 cm for 1, 3, 7 and 14 days. The

calcium, silicon, and phosphorus concentrations were analyzed by inductively coupled plasma spectroscopy (ICP). Additionally, Corning pH meter 340 was used to check the pH values after each immersion period.

C. Biological Evaluation

1. Cell Cytotoxicity

In order to evaluate the toxic behavior of the BGs powder and % viability of MC3T3 cells, MTT [3-(4, 5-dimethylthiazol-2-yl)-2, 5-diphenyl tetrazolium bromide] assay was performed. Firstly, MC3T3 cells were seeded at a density of 6×10^3 on BGs in regular DMEM medium and placed in the incubator. Then after 1, 3 and 7 days, the medium was replaced with 100 µL of 5 mg/mL MTT solution (Sigma Aldrich) and incubed for 72 h. Finally, the optical density (OD) values of the dissolved precipitated formazan crystals were measured at a wavelength of 570 nm using a multi-well microplate reader (EL 312e Biokinetics reader, Biotek Instruments).

2. ALP Activity

ALP is a useful differentiation marker for ostosteoblasts expression based on the Lawry et al method [38]. The ALP enzyme kit was used to measure ALP activity according to the manufacturer's instruction (Biocat, Heidelberg, Germany). Briefly, MC3T3-E1 cells were seeded on BGs at a density of 1×10^4 cells.cm^{-2} and cultured for 1, 3 and 7 days in the incubator. After each incubation time, the cell layer was rinsed carefully with phosphate buffered saline (PBS) and followed by addition of 1 ml Tris buffer and 1 ml of a p-nitrophenyl phosphate solution (pNPP, Sigma, 16 mmol.L^{-1}). After 5 min incubation at 30 °C, the liberated p-nytrophenyl was measurement using a microplate reader at 410 nm [39].

3. Live and Dead Cell Staining

The live/dead (L/D) cell assay was used to assess biocompatibility of the synthesized BGs using Live/Dead cell viability kit (Sigma-Aldrich). Briefly, MC3T3-E1 cells were seeded at a density of 15,000 cells.cm^{-2} on 58s and 68s samples. After 1 and 7 days of culture, the BGs with attached cells were rinsed 3 times gently with phosphate buffered saline (PBS) and incubated for an additional 15 min in dark with 200 µL of 2 µM calcein-acetoxymethyl ester (calcein-AM) and 4 µM ethidium homodimer-1 (EthD-1) in a humidified atmosphere of 5% CO_2- 95% air at 37 °C. Finally, the fluorescence microscope (Olympus, USA) with a Zeiss AxioCam digital camera was used to capture representative images of live (green fluorescent) and dead (red fluorescent) MC3T3 cells.

4. Antibacterial Studies

To compare the bactericidal activity of 58s and 68s samples with control (inert SiO_2 with a poor antibacterial effect), at the first step, the MRSA bacteria were diluted approximately to 0.5×10^8 to 2×10^8 mL^{-1} then 0.1 ml bacterial suspension added to the mixture of 0.9 ml LB medium and 10 mg of each BG and followed by 1 h culture at 37 °C. Afterwards, 100 µl of final suspensions were streaked onto LB-agar plates and incubated at 37 °C for 12 h in the dark [27] and eventually the final colony-forming units per milliliter (CFU/mL) were calculated as a bactericidal percentages as follows [27], [28]:

Bactericidal fraction = 1- (number of survived bacteria/number of total bacteria).

D. Statistical Analysis

All of the biological experiments were run in at least three replicate sets. The data were presented as the means ± standard deviation. Furthermore, statistical analyses were done by using GraphPad Prism software package, version 3.0 (GraphPad Prism, USA). A p-value less than 0.05 was considered statistically significant and $^{**}P < 0.01$ and $^{***}P < 0.001$ were considered as a high statistically significant.

III. Results and Discussion

A. BG's Density and Oxygen Density (OD)

Oxygen density is investigated as a measure for the compactness of the BG network [40].

The OD values for synthesized 58s and 68s are given in Table III. Results demonstrated that calculated oxygen density increased in the 68s with respect to 58s due to the more silica (SiO_2) in BG composition as a network former. In the meanwhile, it should be noted that the difference in oxygen density values between 58s and 68s was statistically significant ($^{*}P < 0.05$).

TABLE III
The Oxygen Density of the BG-58s and BG-68s

BG	58s	68s
OD	0.756±0.009	0.776±0.007

B. Phase Analysis and Structural Groups

As it seen in Fig. 1, the characteristic peaks of HA (JCPDS (No. 09-432)) were detected in the XRD patterns of 58s and 68s after 7 days of immersion in SBF solution while, before immersion in the SBF, because of their amorphous structure, no characteristics peak in their XRD patterns were observed (not shown).

The appearance of peaks at 2 theta equal to 25.8° and 31.8° assigned to (200) and (211) planes on 7th day of immersion in SBF, confirmed the formation of crystalline HA on the surfaces. By increasing the immersion time to 14 days, two mentioned peaks became more pronounced. Meanwhile, the maturity of the formed HA layer on 58s approved by detection of the two new peaks at 2 theta equal to 32.18° and 32.86° attributed to the crystallization of (112) and (300) atomic planes in apatite lattice respectively [41]. XRD results revealed that both 58s and 68s had *in vitro* bioactivity. However, 58s had relatively higher HA formation ability. In the other words, 58s had relatively higher *in vitro* bioactivity than 68s.

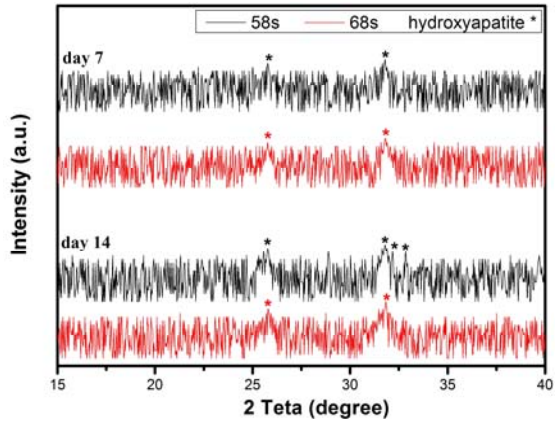

Fig. 1 The XRD patterns of BG-58s and BG-68s after 7 and 14 days soaking in SBF

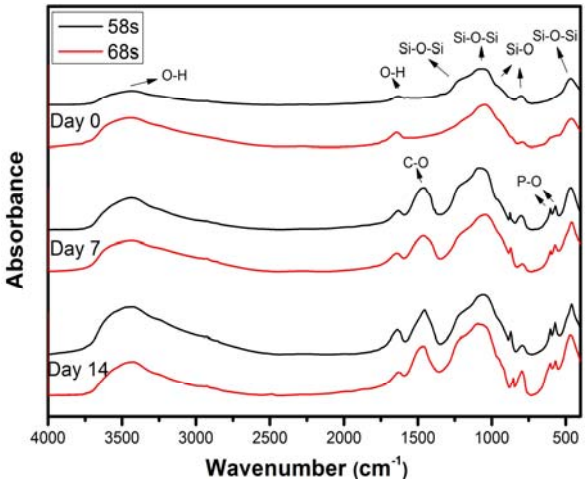

Fig. 2 The FTIR spectra of BG-58s and BG-68s, before (day 0) and after different soaking after 7 and 14 days

The FTIR spectra of 58s and 68s before (day 0) and after soaking in SBF for 7 and 14 days are presented in Fig. 2. Before soaking in SBF, the stretching and bending vibrations of Si–O–Si were observed in FTIR spectra of both BGs. The detected peak near 470, 790, 1000–1100 and 1250 cm^{-1} were respectively corresponded to the bending vibration of Si–O–Si [42], the symmetric stretching of Si–O, the Si–O–Si symmetric stretching and Si–O–Si asymmetric stretching [43]. By increasing the immersion time to 7 days, phosphate absorption bands related to the asymmetric bending mode of PO_4^{3-} group were detected at 603 and 570 cm^{-1} are characteristic band of phosphate in crystalline phases [7]. In addition, appearance the bands at 870 and 1455 cm^{-1} attributed to the C–O stretching in carbonate groups substituted for phosphate groups in apatite lattice [44], [45] and also, two appeared bands at 3500 and 1651 cm^{-1} were related to the stretching mode of the OH group [46]. Detection P–O and C–O bands in FTIR spectra of 58s and 68s confirmed the formation of a calcium phosphate on their surfaces after 7 days of immersion in SBF. The intensity of mentioned peaks increased from 7th to 14th day of immersion. While, 58s exhibited peaks with more intensity compared to the BG-68s.

FTIR results were in good accordance with XRD results that approved the formation of HA on 58s and 68s surfaces after immersion in SBF for 7 days.

C. Ion Chemistry of SBF Solution

Figs. 3 (a)-(d) illustrates the changes in ionic concentration of Ca, Si and P in the SBF and the pH values with immersion time for 1, 3, 7, and 14 days. As it seen in Fig. 3 (a), the Ca concentrations in SBF solution for 58s sand 68s increased rapidly from 100 ppm to 300 and 265 ppm, respectively. This stage was occurred because of the cationic exchange and ionic release from the BGs surfaces into the SBF solution in the first stage of HA formation that previously described. On day 3rd of immersion, the mentioned Ca concentration values of 58s sand 68s sharply decreased to about 130 and 158 ppm, respectively, probably due to the initiation of calcium phosphate compounds precipitation. By comparison the trends of Ca concentration change in 58s and 68s, it was revealed that more Ca released from 58s compared to 68s. Meanwhile, the sharper decreasing of Ca concentration values due to HA formation, confirmed higher *in vitro* bioactivity of 58s in comparison with 68s.

Fig. 3 (b) demonstrated that Si had similar trend to Ca. As it obvious, Si release was decreased by increasing the SiO_2 content in the BG composition due to the higher oxygen density. Consequently, on first day of immersion, treated SBF solution with 58s showed higher Si content in compared with 68s. On the other hand, by increasing the immersion time up to 14 days, Si concentrations decreased due to precipitation of Si in a form of SiO_2 rich sub-layer on the surface of BGs.

Fig. 3 (c) exhibited that P concentration continuously decreased during the immersion, which showed consumption of this ion for HA formation and can be used as an estimation for the rate of HA precipitation. It could be understood from Fig. 3 (c) that 68s had higher P concentration in the SBF compared to 58s due to a lower HA formation rate.

The pH variation of SBF as a function of immersion time is shown in Fig. 3 (d). It can be seen that the pH values of SBF solution increased rapidly due to the ion exchange between Ca^{2+} and H^+ ions from the BG and SBF, respectively. Fig. 4 (d) showed that 58s had higher pH values in comparison with BG-68s because of its higher ionic exchange due to its lower network connectivity.

Altogether, ICP-AES results were in reasonable agreement with oxygen density results that confirmed 58s with lower oxygen density had higher solubility than 68s.

D. Surface Morphology

In vitro bioactivity of the synthesize BGs was studied in SBF solution for different time period up to 14 days. Fig. 4 shows the SEM morphology of 58s and 68s surfaces before and after immersion in SBF for 7 and 14 days. As it seen before immersion (Figs. 4 (a) and (d)), no spherical HA was observed on their surfaces.

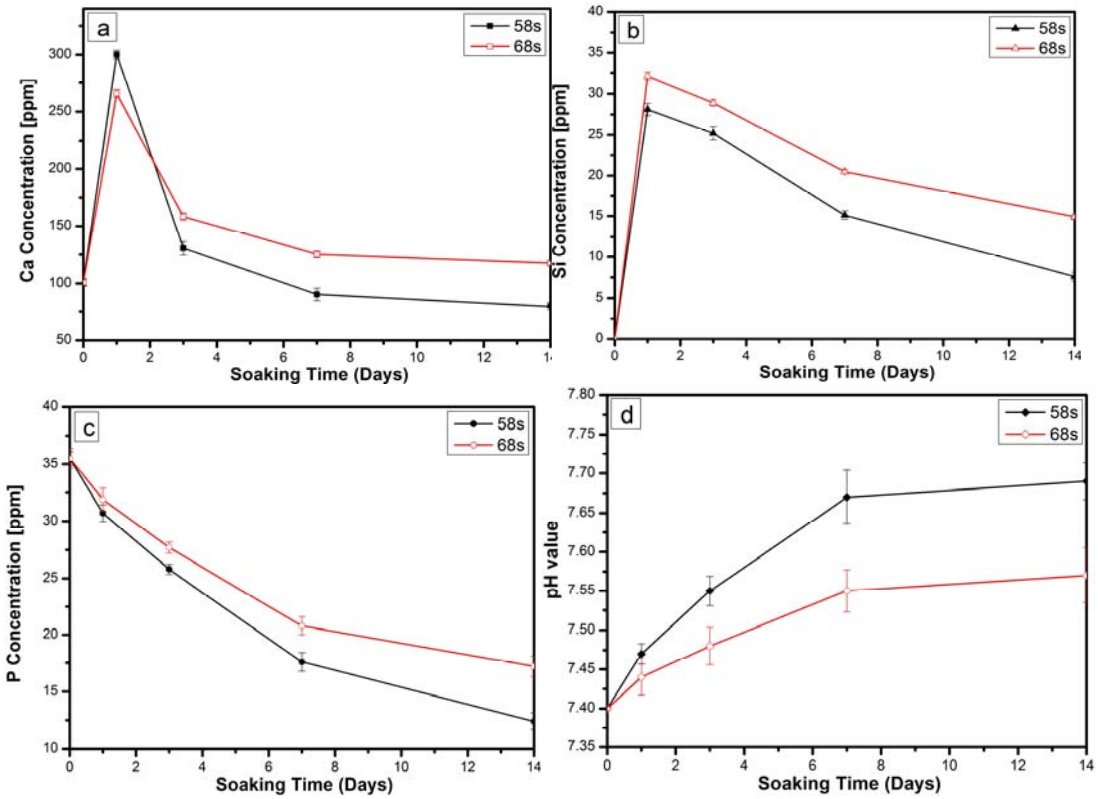

Fig. 3 Variation of elemental concentration and pH in the SBF over soaking time for calcium (a), silicon (b), phosphorus (c), pH (d)

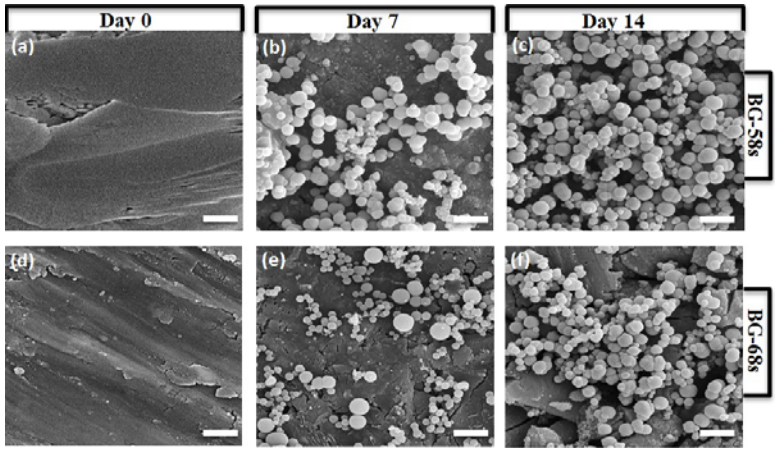

Fig. 4 SEM morphology of the 58s and 68s surfaces before and after soaking in the SBF for 7 and 14 days. Scale bar represents 2 μm in all images

After one day of immersion in SBF, small spherical aggregates of the HA were formed on the surface of the BGs (Figs. 4 (b) and (e)), while 58s showed relatively higher HA formation capability than 68s which was in good agreement with the intensities of the characteristic peaks of HA in their XRD patterns. With increasing the time of immersion to 14 days, the amount of precipitated HA increased for both of the 58s and 68s. Meanwhile, the surface of 58s was fully covered by small spherical aggregates of HA while, 68s surface was partially covered by a relatively less amount of small spherical particles. The relatively lower bioactivity of 68s may be attributed to a lower rate of nucleation as a result of lower supersaturation of the groups that are responsible for HA formation. This result was in reasonable agreement with Si and Ca ion release rate (ICP-AES result) that was discussed in the previous section (Figs. 3 (a) and (b)).

E. In vitro Biological Evaluation

1. Live/Dead Assay

The fluorescent images of the live/dead MC3T3-Es cells after culturing for 1 and 7 days on the surface of 58s and 68s are present in Fig. 5. After 1 day of culture, 58s and 68s demonstrated nearly the same staining pattern with confluent green fluorescent live cells and a relatively sparse numbers of

red fluorescent dead cells. As it seen, with increasing the culture time to 7 days, the mean number of live cells increased compared to the 1st day of culture for both 58s and 68s. Meanwhile, live/dead assay was in good accordance with

MTT results (Fig. 6). Taken together, the *in vitro* live/dead cell assay provided additional evidence that the 58s and 68s possess nearly similar and acceptable biocompatibility.

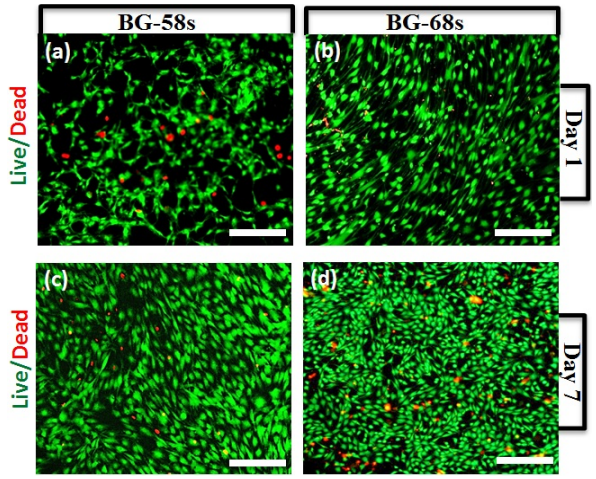

Fig. 5 Two dimensional (2D) MC-3T3 cells cultured in presence of BG-58s andBG-68s. Representative live/dead fluorescence images of MC-3T3 cells cultured on BG-58s (a, c) and BG-68s (b, d) after 1 and 7 days of culture respectively. Green fluorescent cells are alive and red Fluorescent cells indicate dead cells. Scale bar represents 100 μm in all images

2. Cell Proliferation

Fig. 6 shows the proliferation of the MC3T3-E1 osteoblastic cells cultured on 58s and 68s for 1, 3 and 7 days. On 1st day of culture, no significant difference was observed in formation of formazon between the control, 58s and 68s samples ($^{*}P>0.05$). While, by increasing the culture time to 3 days, both 58s and 68s showed statistically significant higher optical density (OD) values compared to the control ($^{*}P<0.05$). Meanwhile, there was no statistically significant difference between BG-58s and BG-68s ($^{*}P>0.05$). As seen in Fig. 6, after 7 days of culture, MC3T3-E1 cells on surface of both 58s and 68s were reached to their maximum proliferation on day 7 without statistically significant difference between (*P>0.05). Meanwhile, Tavakolizadeh et al. previously reported the significant increase in the population and activity of viable unrestricted somatic stem cell (USSC) in presence of 58s [47].

Our MTT results revealed that not only 58s and 68s were biocompatible (have not toxicity) but also both of them exhibited a statistically significant increase in proliferation of MC3T3-E1 cells. In other words, presence of more CaO in composition of sol-gel derived SiO_2–CaO–P_2O_5 ternary system (36 mol % in 58s vs. 26 mol % in 68s) had no significant positive effect on MC3T3-E1 cells proliferation.

3. ALP Activity

The ALP activity of MC3T3-E1s, cultured on BG-58s and BG-68s after 1, 3 and 7 days are presented in Fig. 7. As it is observed, ALP activities of MC3T3-E1 cells increased on both BG-58s and BG-68s with the increase of culture time from 1 to 7 days. On first day of culture, the levels of ALP were not statistically significant different for 58s and 68s (*P>0.05). After 3 days of culture, the ALP activity of MC3T3-E1s in presence of 58s and 68s enhanced approximately 2 times compared to day 1. Meanwhile, on day 3rd, the maximum ALP activity level was attributed to the 58s with statistically significant difference ($^{*}P<0.05$) in comparison with control while, there was no significant difference observed between BG-68s and control (*P>0.05). Finally, after 7 days of culture, both 58s and 68s showed significant enhancement for differentiation of MC3T3-E1s compared to the control ($^{*}P<0.05$) with no difference between them (*P>0.05). According to the MTT and ALP activity results, 58s had relatively higher proliferation and osteoblastic activity of the MC3T3-E1s with respect to 68s.

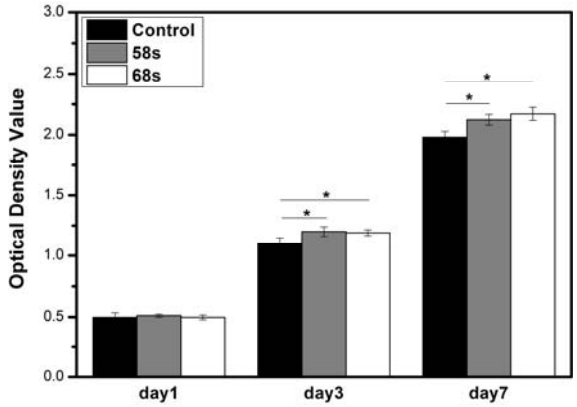

Fig. 6 The proliferation of the osteoblast-like cell line, MC3T3-E1, cultured on BG-58s and BG-68s for 1, 3 and 7 days. (*P < 0.05, **P < 0.01 and ***P < 0.001)

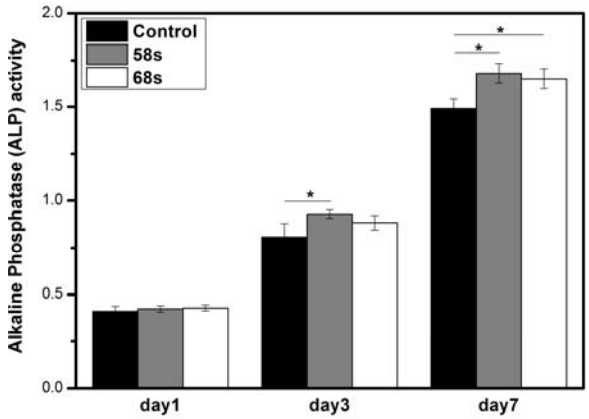

Fig. 7 The ALP activity of the osteoblast-like cell line, MC3T3-E1, cultured on BG-58s and BG-68s for 1, 3 and 7 days. (*P < 0.05, **P < 0.01 and ***P < 0.001)

4. Antibacterial Studies

The bactericidal percentage of synthesized BG-58s and BG-68s is shown in Fig. 8. As it is observed, both 58s and 68s showed a remarkable bactericidal effect against MRSA bacteria in compared with control (at fixed 0.01 $g.mL^{-1}$ concentration). The 68s sample showed statistically significant

increase in bactericidal efficiency against MRSA bacteria ($^{**}P<0.01$), while 58s exhibited highly significant difference than control ($^{***}P<0.001$).

The exact mechanism of bactericidal effect of BGs has not discovered yet [48]. But, previous studies reported that the presence of calcium [48], phosphate [48] as well as the higher pH values [27] may be responsible for antibacterial property of BGs.

Taken together, antibacterial studies revealed that BG-58s had more significant antibacterial effect against MRSA bacteria in comparison with 68s ($^{*}P<0.05$) due to the higher concentration of Ca and P ions in the SBF solutions (ICP-AES data; Figs. 3 (a) and (c)) as well as the higher pH values (Fig. 3 (d)).

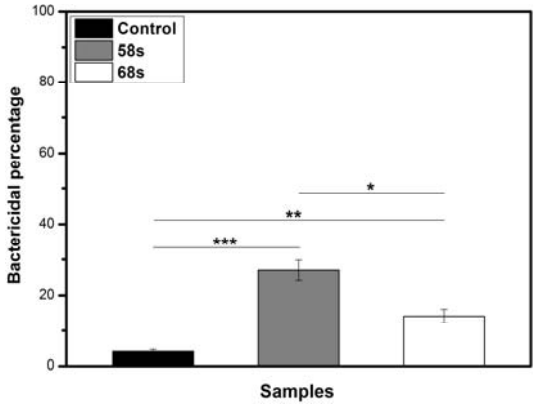

Fig. 8 The bactericidal percentages of 10 mg/ml of inert SiO_2 (as a control), BG-58s and BG-68s

IV. Conclusions

The effects of CaO content in two series of synthesized sol-gel derived BG in SiO_2–CaO–P_2O_5 ternary system on *in vitro* bioactivity, MC3T3 cells cytotoxicity and proliferation as well as antibacterial efficiency have been investigated. It was found that dissolution rate decreased with increasing oxygen density of the BG from 58s to 68s. In addition, XRD and FTIR analysis demonstrated the *in vitro* bioactivity was retarded in presence of less CaO in BG-68s composition with respect to BG-58s. Moreover, ICP-OES data revealed that the higher amount of CaO and SiO_2 in SiO_2–CaO–P_2O_5 BG resulted in an increase and a decrease in the solubility of 58s and 68s, respectively and was attributed to their oxygen density. Therefore, the lower bioactivity of 68s compared with 58s was possibly justified by its lower supersaturation degree that could induce a lower rate of nucleation and growth of the HA on its surfaces.

Both 58s and 68s had no cytotoxicity effect on MC3T3-E1cells. In the meanwhile, live/dead assay qualitatively exhibited that on 1st day of culture, 58s and 68s had nearly the same staining pattern which confirmed their acceptable biocompatibility, and also after 7 days of culture, the cells on the 58s proliferated and reached almost to a confluence level with relatively lower proportion of dead cells in comparison to the 68s. Furthermore, both 58s and 68s showed antibacterial efficiency against MRSA bacteria while, 58s had a statistically significant difference in comparison with BG-68s ($^{*}P < 0.05$).

Taken together, the CaO content in SiO_2–CaO–P_2O_5 ternary system was more effective to facilitate higher *in vitro* bioactivity, cell proliferation and differentiation. Eventually, 58s BG (mol%: 60%SiO_2–36%CaO–4%P_2O_5) with higher *in vitro* bioactivity and bactericidal effect is considered as a promising candidate for further modifying and functionalizing for delivery of therapeutic ions and drug/growth factors such as bone morphogenetic protein (BMP), vascular endothelial growth factor (VEGF) and dexamethasone, etc., to stimulate bone tissue regeneration and remodeling.

RENCEEEFR

[1] L. L. Hench, The story of Bioglass®, J. Mater. Sci. Mater. Med. 17 (2006) 967–978.
[2] L. L. Hench, Bioceramics: From Concept to Clinic, J. Am. Ceram. Soc. 74 (1991) 1487–1510.
[3] P. Saravanapavan, J. R. Jones, R. S. Pryce, L. L. Hench, Bioactivity of gel-glass powders in the CaO-SiO2 system: A comparison with ternary (CaO-P2P5-SiO2) and quaternary glasses (SiO2-CaO-P2O5-Na2O), J. Biomed. Mater. Res. 66A (2003) 110–119.
[4] T. Kokubo, Apatite formation on surfaces of ceramics, metals and polymers in body environment, Acta Mater. 46 (1998) 2519–2527.
[5] F. Sharifianjazi, N. Parvin, M. Tahriri, Formation of apatite nano-needles on novel gel derived SiO2-P2O5-CaO-SrO-Ag2O bioactive glasses, Ceram. Int. 43 (2017) 15214–15220.
[6] X. Lu, L. Deng, C. Huntley, M. Ren, P.-H. Kuo, T. Thomas, J. Chen, J. Du, Mixed Network Former Effect on Structure, Physical Properties, and Bioactivity of 45S5 Bioactive Glasses: An Integrated Experimental and Molecular Dynamics Simulation Study, J. Phys. Chem. B. 122 (2018) 2564–2577.
[7] M. Mozafari, F. Moztarzadeh, M. Tahriri, Investigation of the physico-chemical reactivity of a mesoporous bioactive SiO2–CaO–P2O5 glass in simulated body fluid, J. Non. Cryst. Solids. 356 (2010) 1470–1478.
[8] R. Gupta, A. Kumar, Bioactive materials for biomedical applications using sol–gel technology, Biomed. Mater. 3 (2008) 34005.
[9] L. L. Hench, Biomaterials: a forecast for the future, Biomaterials. 19 (1998) 1419–1423.
[10] M. Vallet-Regí, A. J. Salinas, D. Arcos, From the bioactive glasses to the star gels, J. Mater. Sci. Mater. Med. 17 (2006) 1011–1017.
[11] P. Sepulveda, J. R. Jones, L. L. Hench, Characterization of melt-derived 45S5 and sol-gel-derived 58S bioactive glasses, J. Biomed. Mater. Res. 58 (2001) 734–740.
[12] N. Li, Q. Jie, S. Zhu, R. Wang, Preparation and characterization of macroporous sol–gel bioglass, Ceram. Int. 31 (2005) 641–646.
[13] P. Sepulveda, J. R. Jones, L. L. Hench, In vitro dissolution of melt-derived 45S5 and sol-gel derived 58S bioactive glasses, J. Biomed. Mater. Res. 61 (2002) 301–311.
[14] A. Perardi, M. Cerrruti, C. Morterra, Carbonate formation on sol-gel bioactive glass 58S and on Bioglass® 45S5, Stud. Surf. Sci. Catal. 155 (2005) 461–469.
[15] K. Ohura, T. Nakamura, T. Yamamuro, T. Kokubo, Y. Ebisawa, Y. Kotoura, M. Oka, Bone-bonding ability of P2O5-Free CaO · SiO2 glasses, J. Biomed. Mater. Res. 25 (1991) 357–365.
[16] J. Zhong, D. C. Greenspan, Processing and properties of sol-gel bioactive glasses, J. Biomed. Mater. Res. 53 (2000) 694–701.
[17] J. R. Jones, Review of bioactive glass: From Hench to hybrids, Acta Biomater. 9 (2013) 4457–4486.
[18] L. L. Hench, J.R. Jones, Bioactive Glasses: Frontiers and Challenges., Front. Bioeng. Biotechnol. 3 (2015) 194.
[19] J. Ye, J. He, C. Wang, K. Yao, Z. Gou, Copper-containing mesoporous bioactive glass coatings on orbital implants for improving drug delivery capacity and antibacterial activity, Biotechnol. Lett. 36 (2014) 961–968.
[20] A. Moghanian, S. Firoozi, M. Tahriri, Characterization, in vitro bioactivity and biological studies of sol-gel synthesized SrO substituted 58S bioactive glass, Ceram. Int. 43 (2017).
[21] A. Moghanian, S. Firoozi, M. Tahriri, Synthesis and in vitro studies of sol-gel derived lithium substituted 58S bioactive glass, Ceram. Int. 43 (2017) 12835–12843.

[22] A. Moghanian, A. Sedghi, A. Ghorbanoghli, E. Salari, The effect of magnesium content on in vitro bioactivity, biological behavior and antibacterial activity of sol–gel derived 58S bioactive glass, Ceram. Int. (2018).
[23] I.A. Silver, J. Deas, M. Erecińska, Interactions of bioactive glasses with osteoblasts in vitro: effects of 45S5 Bioglass®, and 58S and 77S bioactive glasses on metabolism, intracellular ion concentrations and cell viability, Biomaterials. 22 (2001) 175–185.
[24] A. Moghanian, S. Firoozi, M. Tahriri, A. Sedghi, A comparative study on the in vitro formation of hydroxyapatite, cytotoxicity and antibacterial activity of 58S bioactive glass substituted by Li and Sr, Mater. Sci. Eng. C. 91 (2018) 349–360.
[25] J. Liu, S. C. F. Rawlinson, R. G. Hill, F. Fortune, Strontium-substituted bioactive glasses in vitro osteogenic and antibacterial effects, Dent. Mater. 32 (2016) 412–422.
[26] G. J. Moran, R. N. Amii, F. M. Abrahamian, D. A. Talan, Methicillin-resistant Staphylococcus aureus in community-acquired skin infections., Emerg. Infect. Dis. 11 (2005) 928–30.
[27] S. Hu, J. Chang, M. Liu, C. Ning, Study on antibacterial effect of 45S5 Bioglass®, J. Mater. Sci. Mater. Med. 20 (2009) 281–286.
[28] S. Hu, C. Ning, Y. Zhou, L. Chen, K. Lin, J. Chang, Antibacterial activity of silicate bioceramics, J. Wuhan Univ. Technol. Sci. Ed. 26 (2011) 226–230.
[29] F. Sharifianjazi, N. Parvin, M. Tahriri, Synthesis and characteristics of sol-gel bioactive SiO2-P2O5-CaO-Ag2O glasses, J. Non. Cryst. Solids. 476 (2017) 108–113.
[30] A. Balamurugan, G. Sockalingum, J. Michel, J. Fauré, V. Banchet, L. Wortham, S. Bouthors, D. Laurent-Maquin, G. Balossier, Synthesis and characterisation of sol gel derived bioactive glass for biomedical applications, 2006.
[31] I. A. Silver, J. Deas, M. Erecińska, Interactions of bioactive glasses with osteoblasts in vitro: effects of 45S5 Bioglass®, and 58S and 77S bioactive glasses on metabolism, intracellular ion concentrations and cell viability, Biomaterials. 22 (2001) 175–185.
[32] M. Taghian Dehaghani, M. Ahmadian, M. Fathi, Synthesis, Characterization, and Bioactivity Evaluation of Amorphous and Crystallized 58S Bioglass Nanopowders, Int. J. Appl. Ceram. Technol. 12 (2015) 867–874.
[33] R. Li, A. E. Clark, L. L. Hench, An investigation of bioactive glass powders by sol-gel processing, J. Appl. Biomater. 2 (1991) 231–239.
[34] Z. Hong, R. L. Reis, J. F. Mano, Preparation and in vitro characterization of novel bioactive glass ceramic nanoparticles, J. Biomed. Mater. Res. Part A. 88A (2009) 304–313.
[35] D. Arcos, D. C. Greenspan, M. Vallet-Regí, A new quantitative method to evaluate the in vitro bioactivity of melt and sol-gel-derived silicate glasses, J. Biomed. Mater. Res. Part A. 65A (2003) 344–351.
[36] L. Francis, D. Meng, J. C. Knowles, I. Roy, A. R. Boccaccini, Multi-functional P(3HB) microsphere/45S5 Bioglass®-based composite scaffolds for bone tissue engineering, Acta Biomater. 6 (2010) 2773–2786.
[37] D. S. Brauer, R. Brückner, M. Tylkowski, L. Hupa, Sodium-free mixed alkali bioactive glasses, Biomed. Glas. 2 (2016).
[38] H. M. Elgendy, M. E. Norman, A. R. Keaton, C. T. Laurencin, Osteoblast-like cell (MC3T3-E1) proliferation on bioerodible polymers: an approach towards the development of a bone-bioerodible polymer composite material, Biomaterials. 14 (1993) 263–269.
[39] C. E. Yellowley, Z. Li, Z. Zhou, C. R. Jacobs, H. J. Donahue, Functional Gap Junctions Between Osteocytic and Osteoblastic Cells, J. Bone Miner. Res. 15 (2010) 209–217.
[40] M. Tylkowski, D. S. Brauer, Mixed alkali effects in Bioglass® 45S5, J. Non. Cryst. Solids. 376 (2013) 175–181.
[41] S. Shahrabi, S. Hesaraki, S. Moemeni, M. Khorami, Structural discrepancies and in vitro nanoapatite formation ability of sol–gel derived glasses doped with different bone stimulator ions, Ceram. Int. 37 (2011) 2737–2746.
[42] X. Wu, G. Meng, S. Wang, F. Wu, W. Huang, Z. Gu, Zn and Sr incorporated 64S bioglasses: Material characterization, in-vitro bioactivity and mesenchymal stem cell responses, Mater. Sci. Eng. C. 52 (2015) 242–250.
[43] X. Zhang, Y. Wu, S. He, D. Yang, Structural characterization of sol–gel composites using TEOS/MEMO as precursors, Surf. Coatings Technol. 201 (2007) 6051–6058.
[44] A. Rainer, S. M. Giannitelli, F. Abbruzzese, E. Traversa, S. Licoccia, M. Trombetta, Fabrication of bioactive glass–ceramic foams mimicking human bone portions for regenerative medicine, Acta Biomater. 4 (2008) 362–369.
[45] X. Zhao, B. C. Heng, S. Xiong, J. Guo, T. T.-Y. Tan, F. Y. C. Boey, K. W. Ng, J. S. C. Loo, In vitro assessment of cellular responses to rod-shaped hydroxyapatite nanoparticles of varying lengths and surface areas, Nanotoxicology. 5 (2011) 182–194.
[46] M. Ashok, N. Meenakshi Sundaram, S. Narayana Kalkura, Crystallization of hydroxyapatite at physiological temperature, Mater. Lett. 57 (2003) 2066–2070.
[47] A. Tavakolizadeh, M. Ahmadian, M. H. Fathi, A. Doostmohammadi, E. Seyedjafari, A. Ardeshirylajimi, Investigation of Osteoinductive Effects of Different Compositions of Bioactive Glass Nanoparticles for Bone Tissue Engineering, ASAIO J. 63 (2017) 512–517.
[48] D. Khvostenko, T. J. Hilton, J. L. Ferracane, J. C. Mitchell, J. J. Kruzic, Bioactive glass fillers reduce bacterial penetration into marginal gaps for composite restorations, Dent. Mater. 32 (2016) 73–81.